

Cathodoluminescence study of the spatial distribution of electron-hole pairs generated by an electron beam in $\text{Al}_{0.4}\text{Ga}_{0.6}\text{As}$

Eli Mapchan

Jean-Marc Bonard^{a)} and Jean-Daniel Ganière

Institut de Micro- et Optoélectronique, Ecole Polytechnique Fédérale, CH-1015 Lausanne, Switzerland

Brigitte Akamatsu

France Telecom, Centre National d'Etudes des Télécommunications, Paris B, Laboratoire de Bagneux
196 avenue Henri Ravéra, Boîte Postale 107, F-92225 Bagneux Cedex, France

Daniel Araújo

Departamento de Ciencia de Materiales e IM y QI, Universidad da Cádiz, Apartado 40,
E-11510 Puerto Real, Spain

Franz-Karl Reinhart

Institut de Micro- et Optoélectronique, Ecole Polytechnique Fédérale, CH-1015 Lausanne, Switzerland

(Received 16 October 1995; accepted for publication 5 February 1996)

We use the cathodoluminescence mode of a scanning electron microscope to investigate the depth and lateral dependencies of the electron-hole pairs generation by the electron beam in $\text{Al}_{0.4}\text{Ga}_{0.6}\text{As}$ semiconducting material. A multiquantum well structure acts as a detector to measure the relative number of generated minority carriers by their radiative recombination, allowing a direct assessment of the generation volume in the sample. In contrast to electron-beam induced current which was used in former studies, the method avoids the effect of carrier diffusion for direct band gap materials. This novel technique can be readily applied to other III-V and II-VI semiconductors. The results may be used for the quantitative interpretation of cathodoluminescence and electron-beam induced current measurements. © 1996 American Institute of Physics. [S0021-8979(96)03210-4]

BIB

USES MCSET

I. INTRODUCTION

A very marked trend may be observed in the development of semiconductor structures: they are becoming more and more complex, while their size is reduced at the same time. "Nanostructures" are now a lively field of research, which calls for adapted characterization techniques. Among these, the cathodoluminescence¹ (CL) and electron-beam induced current² (EBIC) imaging and measurement modes in the scanning electron microscopes (SEM) are now widely used and have proven to be powerful tools for the microscale and nanoscale study of semiconductors. However, very few quantitative studies have been published up-to-now (see section II C), principally because the quantitative interpretation of the CL and/or EBIC intensities is difficult to achieve. One of the reasons is the lack of information about the spatial dependence of the energy loss of the electron beam during its interaction with the sample.

The volume defined by all the trajectories of the incident electrons in the sample is generally called the "interaction" or "generation" volume, and it has been studied both experimentally and theoretically. Its shape and dimensions depend on the energy and incidence angle of the beam as well as on the atomic number of the sample. We will use in the following the expression "generation volume" only for the volume where electron-hole pairs are generated by the beam.

We will briefly outline the results of former studies on the subject in section II, and present the method and its application to $\text{Al}_{0.4}\text{Ga}_{0.6}\text{As}$ in section III. Sections IV and V will be devoted to the presentation and discussion of our results on the depth, respectively lateral, dependence of electron-hole (e-h) pairs generation.

^{a)}Electronic mail: jean-marc.bonard@epfl.ch

II. INTERACTION OF THE ELECTRON BEAM WITH THE SAMPLE

A. Experimental studies

Grün³ presented in 1957 the first experience on the energy loss of the beam by studying the luminescence excited by the electrons in low pressure gases (a similar study was performed by Cohn and Caledonia⁴ in 1970). Other authors used materials like fluorescent crystals and photoresist, or studied the transmitted electrons through thin solid targets.

The few direct experimental studies of the depth and lateral dependence in bulk dense solids were all done on semiconducting samples. Everhart and Hoff published the first study, where they used metal oxide semiconductor (MOS) capacitors with different oxide thicknesses to sample the depth dependence.⁵ Oelgart and Scholz,⁶ Oelgart and Werner,⁷ and later Werner *et al.*⁸ measured the dependence of the EBIC signal in heavily doped (10^{18} – 10^{19} cm^{-3}) indirect-gap materials with short diffusion lengths (0.08–0.18 μm). This method has several drawbacks: (a) the generation volume is only indirectly evaluated, since the measured distribution of carriers is a convolution of both generation and diffusion of electron-hole pairs; (b) the increase of the effective diffusion length of the carriers due to processes of self-absorption and reemission of cathodoluminescence makes the method unsuitable for direct-gap materials; and (c) the width of the detector for the created e-h pairs (in this case a *p-n* junction) is quite large (typically, more than 0.3 μm), thus reducing the resolution of the measurement. Konnikov *et al.*⁹ prevented the diffusion of the carriers by detecting the e-h pairs with a layer of wide-band gap material where a *p-n* junction was located: the heterojunctions between the probed narrow-gap material and the detector prevented carrier diffusion into the detector.

3. Theoretical studies and analytical descriptions of the generation volume

The theoretical results are all derived from Monte Carlo simulations, and a semi-empirical function characterizing the simulated interaction is often presented. These expressions, giving the spatial dependence of the energy dissipation or of the carrier generation rate (the two types of results being in first approximation proportional¹⁰), are usually represented by a product of two functions normalized to unity: a function representing the depth dependence and a function describing the lateral dependence, with the space coordinates normalized to a beam energy and material dependent penetration range.^{1,3}

It is important to point out that the energy needed for the generation of an e-h pair by a high-energy (compared to the band gap energy, E_g) electron is not well known. Studies dating back to the 1960's indicate that the mean energy needed is roughly 3 to 4 E_g , and that this value is independent of the electron energy.^{11,12} These results have to be considered with care: first, the "mean energy" is calculated as the ratio of the energy loss of the electron to the number of created e-h pairs (detected by the current induced at a wide p - n junction in Ref. 12). It is, therefore, not the ionization energy, but it corresponds to a mean energy loss per created e-h pair that includes the energy loss induced by other interaction processes. Second, there was no thorough study of the dependence of the mean energy loss with the energy of the incident electrons: it can be expected to vary since the ionization cross-sections depend also on the energy of the electrons.

The first proposed functions describe the depth dependence only: Everhart and Hoff presented a third-order polynomial function,⁵ while Kyser and Wittry proposed a shifted Gaussian (cited in Ref. 13). Later studies include also the lateral dependence and propose functions composed of one or several Gaussians, with widths that vary with the penetration range (and for some with beam diameter and depth in the sample). Among the most common are the results of Fitting *et al.*¹⁴ and Donolato¹⁰ (function with one Gaussian); Werner *et al.*⁸ and Konnikov *et al.*⁹ (function with two Gaussians, the first one describing the effect of the beam penetrating the sample, and the second one taking into account the contribution of the electrons after multiple scattering events); and finally Akamatsu *et al.*¹⁵ who suggested an expression involving three Gaussians with widths dependent on the beam energy only.

Figure 1 shows the depth (a) and the lateral (b) dependence in $Al_{0.4}Ga_{0.6}As$ of the e-h pair generation, for a detector width of 50 nm and a beam diameter of 30 nm. Figure 1(a) compares the curves predicted by the expressions of Everhart and Hoff,⁵ Werner *et al.*,⁸ Konnikov *et al.*⁹ and Akamatsu *et al.*¹⁵ This comparison reveals great variations in the generation profiles: the expressions of Konnikov *et al.* and Akamatsu *et al.* give very similar results, except near the surface. The maximum of generation at 20 keV is around $z = 0.25$ mm, while Werner *et al.* and Everhart and Hoff predict a far greater penetration in the material. Similar results are obtained for other beam energies between 5 keV and 40 keV.

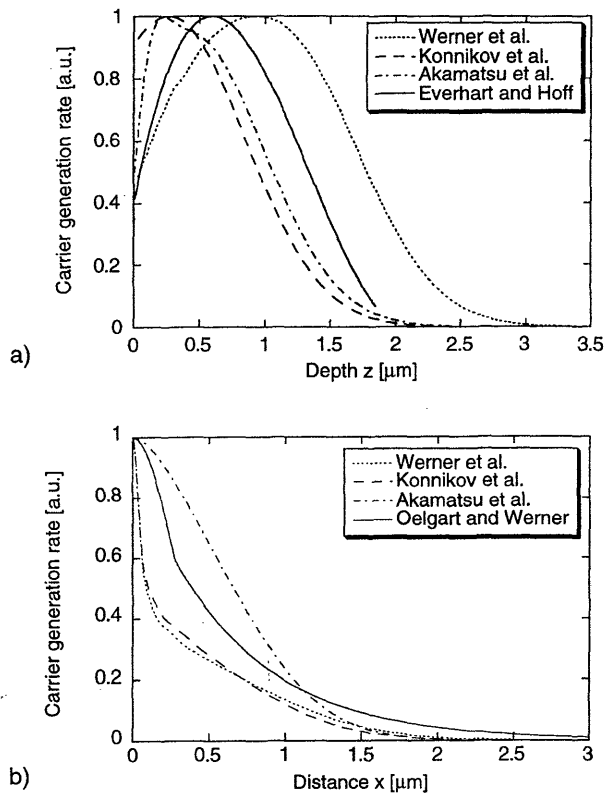


FIG. 1. Depth (a) and lateral (b) dependence of the e-h pairs generation (at 20 keV) in $Al_{0.4}Ga_{0.6}As$ normalized to the maximum of generation, as predicted by the expressions of Akamatsu *et al.* (dash-dotted line), Konnikov *et al.* (dashed line), Werner *et al.* (dotted line) as well as Everhart and Hoff (plain line, depth dependence only) and Oelgart and Werner (plain line, lateral dependence only). The detector width is set to 50 nm, the beam diameter to 30 nm.

The predictions for the lateral dependence also display great variations, as presented in Fig. 1(b). The expressions of Werner *et al.*, Konnikov *et al.*, and Akamatsu *et al.* are compared along with the fit suggested by Oelgart and Werner⁷ on their experimental data for $GaAs_{0.35}P_{0.65}$ (which has a density $\rho = 4.4$ g cm^{-3} comparable to $Al_{0.4}Ga_{0.6}As$). All the profiles but Akamatsu's display a sharp needle-like peak, which is nearly energy independent. This needle-like peak was also observed in most experimental studies,⁶⁻⁹ and is understood as the contribution of the electron-hole pairs generated in the first scattering events of the electrons.

Some rare authors have used an analytical function to describe and simulate in more detail EBIC experiences, like Wu and Wittry for Schottky barriers,¹³ Donolato for dislocations¹⁰ and p - n junctions,¹⁶ and Luke *et al.*¹⁷ for the determination of diffusion lengths at p - n junctions. More recent studies, still involving EBIC evaluations, have been published by Luke¹⁸ for the determination of surface recombination velocities at p - n junctions and by Donolato¹⁹ for grain boundaries. There is to our knowledge only one incorporation of the extended generation for CL evaluations, namely by Sieber²⁰ in the case of III-V homolayers (who also considers the case of EBIC evaluations).

These efforts towards a quantitative analysis of CL and EBIC measurements are nevertheless of great importance for

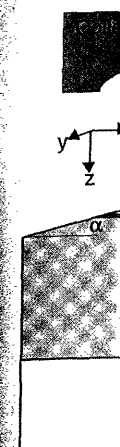


FIG. 2. Experimental setup for e-h pair generation.

the future development of information on the sample.

III. EXPERIMENTAL

A. Instrumentation

The measurements were performed using a scanning electron microscope (SEM), with a detector for the observation of the liquid helium cooled semi-elliptical generation volume (EG&G SP-1500) fiber connected to a photomultiplier equipped with a 50 nm diameter.

In order to avoid the e-h pairs generated in the detector, an efficient detector was used to prevent the detection of the radiative recombination. In this choice, the detection of the quantum yield prevents the detection of the quantum yield.

The structure of the sample is a separate multilayer of $Al_{0.4}Ga_{0.6}As$ on a GaAs substrate. The same material is used for the substrate. The structure is a separate multilayer of $Al_{0.4}Ga_{0.6}As$ on a GaAs substrate.

B. Experimental Results

The dependence of the signal on the angle of the sample is shown in Fig. 3. The angle (inferred from the section). A variation of e-h pairs, of the beam diameter, with the

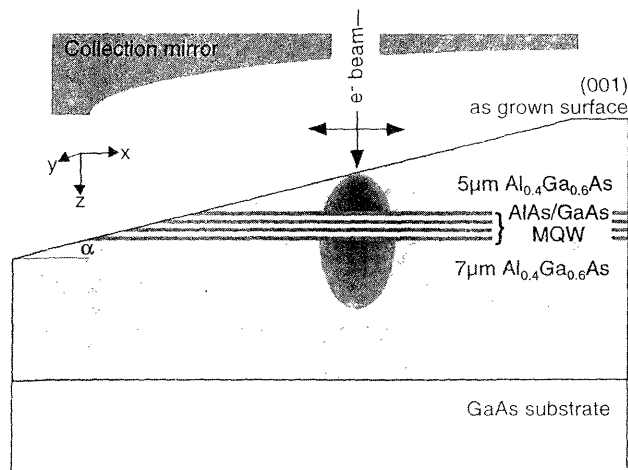


FIG. 2. Experimental setup for the measure of the depth dependence of e-h pairs generation.

the future development of these techniques, and call for more information on the exact shape of the generation volume in the sample.

III. EXPERIMENTAL DETAILS

A. Instrumentation and sample

The measurements are carried out on a Cambridge S-360 SEM, with a modified stage (Oxford Instruments) that allows the observation of the CL in the temperature range between liquid helium and room temperature. The CL is focused by a semi-ellipsoidal mirror on a Si-avalanche photodetector (EG&G SPCM-200), or on the entrance slit of an optical fiber connected to a Jobin-Yvon HR250 monochromator equipped with a Si-CCD camera for spectral acquisition.

In order to measure the spatial distribution of the e-h pairs generated by the electron beam, we have to choose an efficient detector for the created e-h pairs, and we have to prevent the diffusion of the carriers into and out of the detector. In this study, the e-h pairs are detected through their radiative recombination in a multi-quantum well, and a judicious choice for the chemical composition of the barriers prevents the diffusion of the generated carriers into and out of the quantum well.

The structure consists of three GaAs quantum wells of 6 nm separated and enclosed by AlAs barriers of 10 nm. This multi-quantum well (MQW) structure is buried below a 5 μm layer of $\text{Al}_{0.4}\text{Ga}_{0.6}\text{As}$, and a 7 μm thick buffer layer of the same material is grown between the MQW and the GaAs substrate. The whole structure is 10^{16} cm^{-3} Be doped.

B. Experimental setup

The depth dependence is best measured on a sample with an angle lap,⁸ in a setup similar to Fig. 2. The surface of the sample is etched in order to form a lap presenting a small angle (inferior to 0.1°) with the growth surface (see next section). A CL intensity profile proportional to the generation of e-h pairs is then obtained by changing the position, x , of the beam on the surface, and detecting the CL emission with the CCD detector. The probed material is the

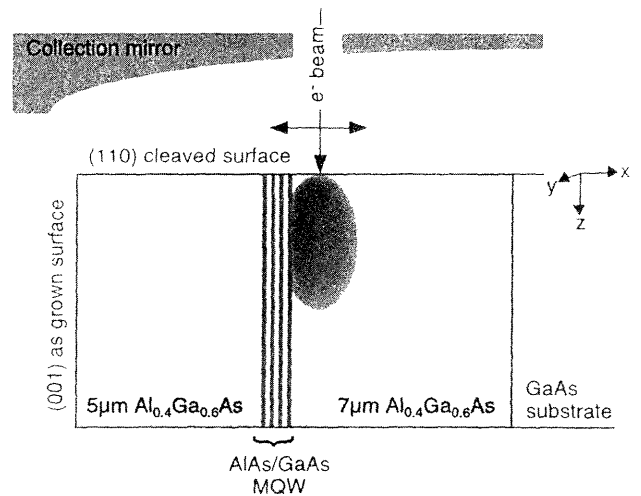


FIG. 3. Experimental setup for the measure of the lateral dependence of e-h pairs generation.

$\text{Al}_{0.4}\text{Ga}_{0.6}\text{As}$ (atomic number $Z=28.7$, density $\rho=4.68 \text{ g cm}^{-3}$, molar weight $A=63.76 \text{ g mol}^{-1}$), where the elastic scattering spreads the incident electron beam. Note that the measure reflects the depth distribution of the generation only if we are in low injection conditions (i.e., if the CL emission is proportional to the beam current, see section III E) and if the collection geometry remains identical through the whole measurement. However, the points of measure are at least 50 μm apart on the sample surface, and the height of the point of impact varies from point to point: this forces us to refocus the beam and the collection mirror before each spectral acquisition.

We presented the results on the lateral dependence in a previous paper.²¹ We will recall here the setup (see Fig. 3) and the main results (in section V). The setup is simpler than for the measure of the depth dependence, and no special preparation of the sample is required. We obtain a CL intensity profile proportional to the generation of e-h pairs by scanning the beam perpendicular to the MQW on the cleaved (110) surface and detecting the CL emission of the MQW with a fixed collection geometry.

The measure of the depth and lateral generation profiles is done at room temperature, for beam energies between 5 keV and 40 keV with a fixed beam current of 500 pA (which corresponds to low injection conditions, as we will see in section III E).

C. Fabrication of the angle lap: method

Angle laps are usually obtained by chemical etching²² [in our case with a 5% bromine (Br)-methanol solution] in a Laub-Garoni "Célestine Proutard" apparatus, like the one depicted in Fig. 4.

A rectangular $3 \times 20 \text{ mm}$ wafer of the sample is fixed on a teflon sample holder, with the left half-side protected with black wax in order to have an intact surface of reference for subsequent depth measurements. The surface is first cleaned with HCl; the sample holder is then placed in the left tube of the apparatus and immersed in methanol. The right tube is filled with the Br-methanol solution. When the valve at the

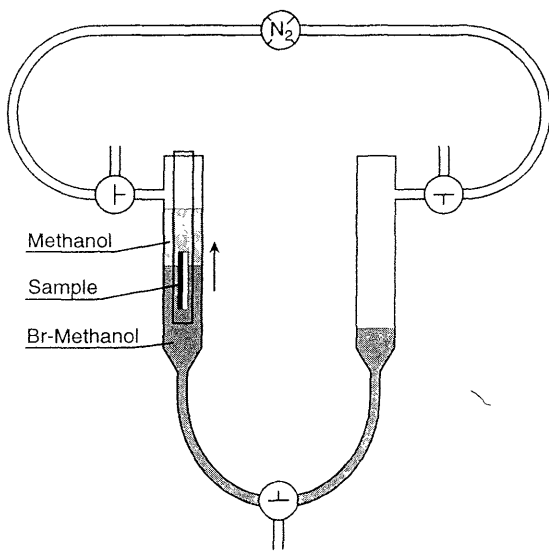


FIG. 4. Schema of the Laub-Garoni "Célestine Proutard" apparatus used for angle lap fabrication. Nitrogen gas is injected in the left or right tube to control the position of the sharp (Br-methanol)-methanol interface.

bottom of the connection joining the two tubes is opened, a sharp methanol-(Br-methanol) interface forms without mixing of the two liquids during the duration of the etching process due to different densities. Nitrogen gas is injected at the top of the right tube to raise the interface, as in Fig. 4; and it is lowered by inverting the two valves situated at the top of the tubes (and, consequently, injecting gas at the top of the left tube). The sample is so progressively attacked, with etching times varying from about 3 minutes at the base of the sample to 0 at the turning point at the top of the sample. When the interface is lowered, the methanol stops the attack and rinses the sample. After the etching, the sample is thoroughly cleaned in methanol.

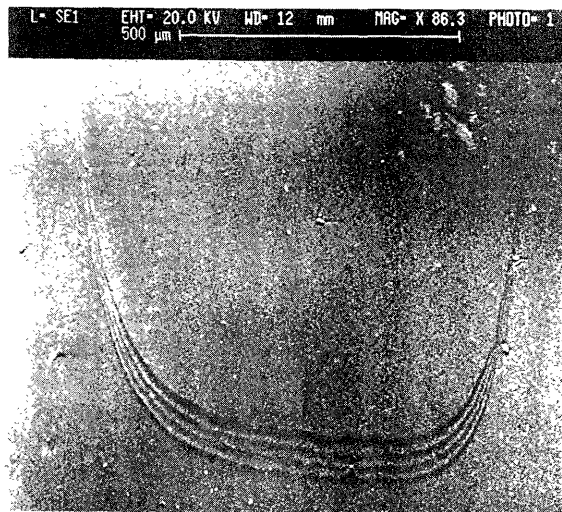


FIG. 5. Scanning electron micrograph of the angle lap, at the location of the intercept of the MQW with the surface of the lap. The AlAs barriers are readily visible (dark contrast).

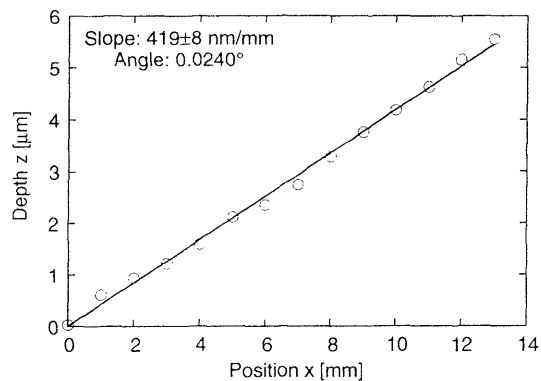


FIG. 6. Depth of attack (in μm) versus position on the angle lap (in mm) for a total attack time of 160 s. The measurement points are indicated with circles, and the corresponding linear fit is marked by the plain line.

D. Fabrication of the angle lap: typical results

The rate of etching and the uniformity of the attack are checked on each angle lap with a Tencor Alpha-Step 200. The profiles show a nearly uniform depth of attack with undulations of less than 20 nm in the centre of the lap, whereas the sides are more attacked.

A SEM micrograph in secondary electrons (SE) mode reveals accurately the result of the etch: Fig. 5 is taken at the location of the intercept of the MQW with the surface of the lap. We can easily see the four AlAs barriers, appearing dark on the micrograph. The difference in depth between the outermost barriers is about 60 nm: the central 500 nm zone of the lap shows here a uniformity in depth of 20 nm, as indicated by the corresponding alpha-step profiles. The border effect is also visible: the etch is far deeper on the sides of the lap.

The angle of the lap is determined by plotting the depth of attack versus the position, as is shown on Fig. 6, and applying a linear regression to obtain the mean slope of the data points, which amounts here to 419 ± 8 nm/mm, corresponding to an angle of 0.0240°.

E. Sample luminescence

Typical CL spectra of the sample at room temperature (like on Fig. 7) show two peaks due to the MQW: the intrinsic luminescence at 1.531 eV and an extrinsic band probably

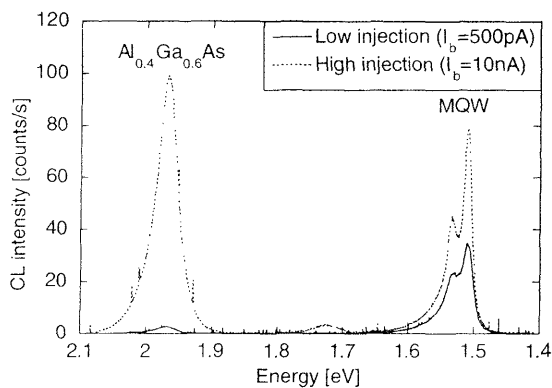


FIG. 7. CL spectra taken at $E_b = 20$ keV, in low injection ($I_b = 500$ pA, plain curve) and high injection ($I_b = 10$ nA, dotted curve) conditions.

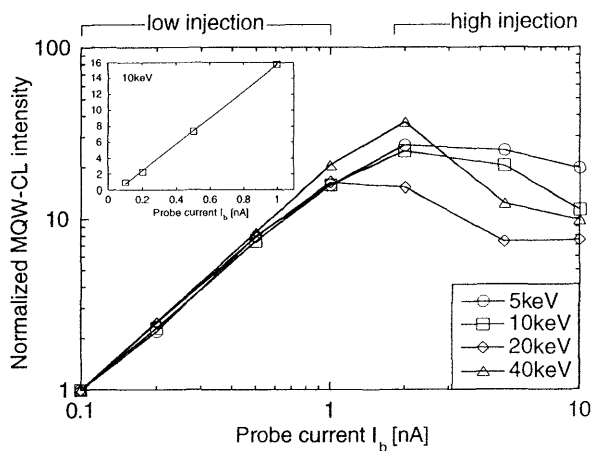


FIG. 8. Normalized MQW-CL intensity versus probe current for different beam energies (circles: 5 keV; squares: 10 keV; diamonds: 20 keV and triangles: 40 keV), with the intensity at $I_b=100$ pA fixed to 1. The inset shows the linear region at 10 keV (squares) and the corresponding linear fit (plain line).

related to the Be acceptors at 1.510 eV. Since an electron beam is used to induce the luminescence, a weak CL emission formed of two peaks associated with the $\text{Al}_{0.4}\text{Ga}_{0.6}\text{As}$ is detected: the band-to-band transition at 1.971 eV and a $30\times$ weaker peak at 1.727 eV due to deep levels. Note on Fig. 7 that the relative intensities of the CL of MQW and $\text{Al}_{0.4}\text{Ga}_{0.6}\text{As}$ vary greatly with the injected current. It is however crucial for the measurement to probe the sample in a current range where the CL emission of the MQW is proportional to the current. To choose our experimental conditions, we acquired spectra on the angle lap (see section III B) at the maximum of generation, for different beam currents and energies. The measurements are summarized on Fig. 8 for beam energies of 5, 10, 20, and 40 keV (both axes are logarithmic). The CL intensity on the y-axis is taken as the area under the MQW peaks, normalized to the area at $I_b=100$ pA for each energy.

The current range where the CL intensity is proportional to the current is situated for all energies between 100 pA (and probably less) and 1 nA. At higher currents, the CL intensity saturates and even diminishes with increasing current. The little inset at the top left of Fig. 8 shows the linear region for $E_b=10$ keV, with a linear fit of the data points. All subsequent acquisitions are done at $I_b=500$ pA for all energies and the CL intensity is always taken as the area under the MQW peaks.

IV. DEPTH DEPENDENCE

A. Depth dependence: experimental results

We present the obtained CL profiles for various beam energies, normalized at the maximum of generation, in Fig. 9. The origin ($z=0$) is taken at the middle of the MQW on the angle lap.

The profiles are reproducible with a precision of at least 100 nm, as verified by measurements taken on different angle laps at 40 keV. The precision increases as the energy

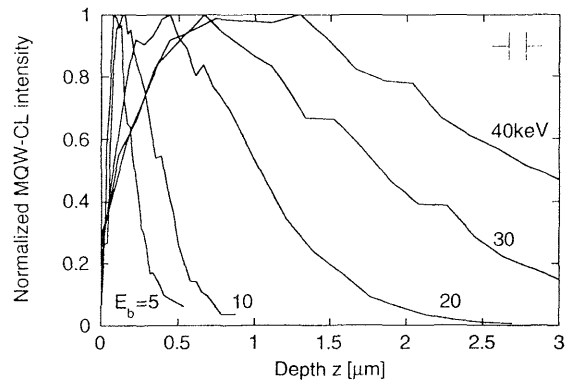


FIG. 9. Depth dependence of the MQW-CL intensity as a function of the depth z of the MQW, for beam energies of 5, 10, 20, 30, and 40 keV. The maximum intensity is fixed to 1. The coordinates are the same as in Fig. 2, and the marker indicates the resolution at 40 keV (100 nm).

decreases, reaching 30 nm at 5 keV: this is quite comparable to the precision obtained for the lateral dependence (50 nm^{21}).

Note that the signal-over-noise ratio of the profiles is quite low, but the shape is easily discernable. As expected, the depth of maximum generation increases with increasing beam energy. This increase is very slow at low beam energies (100 nm at 5 keV to 150 nm at 10 keV), the main feature being the extension of the tail of the profile. The increase of both depth of maximum generation and maximum penetration then rises rapidly with the beam energy. At 40 keV, the maximum of signal is reached at a depth of 1 μm and electron-hole pairs are created down to a depth of 5 μm beneath the surface.

B. Comparison with previous studies

It is interesting to confront our measurements with the results of previous studies. As seen in section II B and on Fig. 1(a), the curves corresponding to the expressions of Akamatsu *et al.* and of Konnikov *et al.* are quite close, while Werner *et al.* and Everhart and Hoff predict a far greater penetration into the sample. We restrict our choice for the comparison to the expression of Akamatsu *et al.* We also include the results given by the Monte Carlo simulation program MC-SET written by Napchan,²³ which uses a single scattering Monte-Carlo model.

Figure 10 displays the measured profiles at 5, 10, 20, and 40 keV (circles joined by dotted line) together with the curves corresponding to the expression of Akamatsu *et al.* (plain line) and the output of the simulation program (dash-dotted line). Akamatsu's model fits our results pretty well for energies above 10 keV, especially around 20 keV. MC-SET however seems to overestimate the penetration in the material for energies superior to 10 keV. At 5 keV, no model or simulation gives a satisfactory approximation to our profile. Indeed the measured increase in penetration depth between 5 keV and 10 keV is far smaller than predicted by all the models.

Another characteristic of the profiles in comparison to the models and simulation is the small CL intensity detected for near zero depths. All models give an intensity of at least

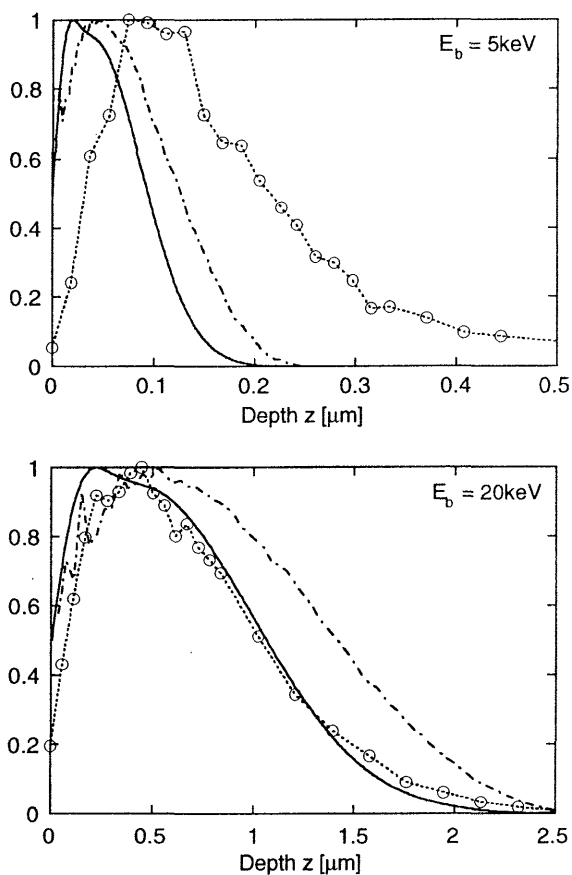


FIG. 10. Depth dependence of the e-h pair generation for beam energies of 5, 10, 20, and 40 keV; as predicted by the expression of Akamatsu *et al.* (plain line), by the simulation program MC-SET (dash-dotted line) and as measured in this work (circles joined by dotted line).

60% of the maximum intensity at $z=0$, while we detect zero depth intensities between 5% and 25% of the maximum intensity, increasing with the beam energy. This stark deviation from the predictions could be provoked by surface recombination effects at the surface of the sample, where the quantum well is apparent on the etched lap. This is however unlikely: at 5 keV, the second measurement point on the profile corresponds to a depth of 20 nm, which means that the e-h pairs are created in the quantum well approximately $50 \mu\text{m}$ in horizontal distance from the surface of the lap. Even with a large diffusion length in the well, only a very small number of carriers may reach the surface before recombination. The outlined effect is therefore probably genuine.

C. Analytical function

It is very useful, for further applications, to deduce an analytical function which describes the measured profiles. As we stated in section II C, most analytical expressions in the literature involve Gaussian functions with widths related to penetration ranges like the Bethe or the Grün range.

We tried to fit our profiles with Gaussian functions, but we could not get a satisfactory agreement. We then settled on a simple function, an exponential multiplied by a parabola and characterized by two parameters Λ and z_0 :

$$I(z) = \frac{\exp[(2\Lambda - z_0)/\Lambda]}{4\Lambda^2} (z + z_0)^2 \exp\left(-\frac{z}{\Lambda}\right). \quad (1)$$

The first factor ensures normalization, so that the maximum of the curve is equal to 1. When $z_0=0$, equation (1) describes a bell shaped curve with a root in $z=0$, the maximum at $z=2 \times \Lambda$ and tending to 0 as z tends towards infinity. A positive z_0 shifts the maximum to $z=2 \times \Lambda - z_0$ and the root to $z_0 = -z_0$, thus leading to a positive y-axis intercept.

Figure 11 shows the value of the parameters Λ (circles) and z_0 (squares) (both in μm) with the beam energy E_b (in keV). The dependence of Λ and z_0 can be written as

$$\Lambda = 0.03 + 0.0015E_b^{1.68}, \quad (2a)$$

$$z_0 = 0.002 \exp(E_b/12.6). \quad (2b)$$

The curves described by equations (2) are drawn as plain (for Λ) and dotted (for z_0) lines in Fig. 11.

The experimental profiles for 5, 10, 20, and 40 keV are displayed along with the curve corresponding to equations (1) and (2) in Fig. 12, to demonstrate the validity of the analytical function for our measurements. The coincidence between analytical and experimental curves is very good, apart from the intensity at $z=0$ which is overestimated and for the 5 keV profile which appears closer to the surface than in the experiment.

Λ [μm]

0.1

0.01

FIG. 11. Dep... error bars gi... function of e... work, along... sponding to e...

Equati... maximum... z_{pen} , defin... the maxim...

$z_{\text{gen}} =$
and

$z_{\text{pen}} =$

FIG. 12. Dep... by the analyti...

0

0

0

0

0

0

0

0

0

0

0

0

0

0

0

0

0

0

0

0

0

0

0

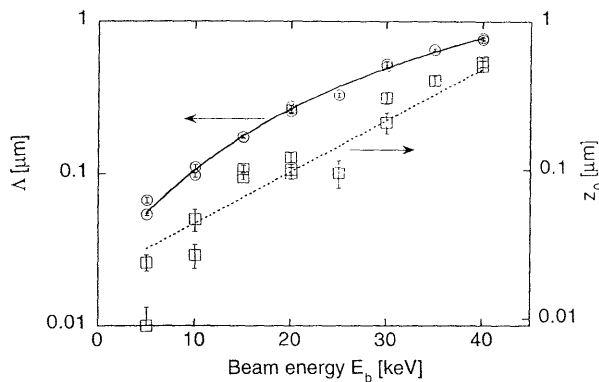


FIG. 11. Dependence on the beam energy of the parameters Δ (circles with error bars giving the error of the fit) and z_0 (squares) of the analytical function of equation (1) describing the depth dependence measured in this work, along with the curves (plain line for Δ and dotted line for z_0) corresponding to equations (2a) and (2b).

Equations (2) also allow one to estimate the depths of maximum generation z_{gen} and of maximum penetration z_{pen} , defined arbitrarily where the intensity is down to 1% of the maximal intensity. We, therefore, have

$$z_{\text{gen}} = 2\Delta - z_0 \quad (3)$$

and

$$z_{\text{pen}} = 10\Delta - z_0. \quad (4)$$

TABLE I. Depths of maximum generation z_{gen} and maximum penetration z_{pen} in function of the beam energy E_b calculated from equations (3) and (4), compared to the Grün range R_g .

E_b [keV]	z_{gen} (μm)	z_{pen} (μm)	R_g (μm)
5	0.08	0.49	0.17
10	0.16	0.97	0.57
15	0.28	1.65	1.16
20	0.43	2.50	1.92
25	0.58	3.51	2.84
30	0.75	4.63	3.90
40	1.06	7.20	6.46

Table I lists the values of both depths along with the Grün range, which is frequently used as an approximation for the penetration depth of the beam in a material,^{1,3} for various beam energies. The Grün range is comparable to the depth of maximum penetration for energies greater than 20 keV, but again underrates greatly the penetration of the electron for small beam energies.

As a comment to this result, the main difference between our measurements and former studies is that the generation volume does not shrink to a point as the beam energy is decreased: this is reflected by the fact that both parameters of our analytical function do not tend towards zero with decreasing energy. The first reason for this comes from the experimental conditions, since the width of the detector is

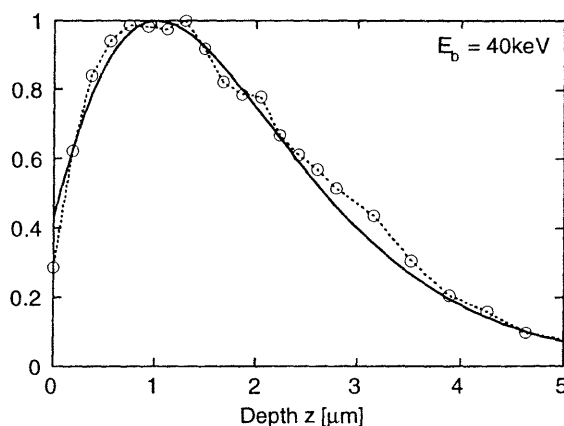
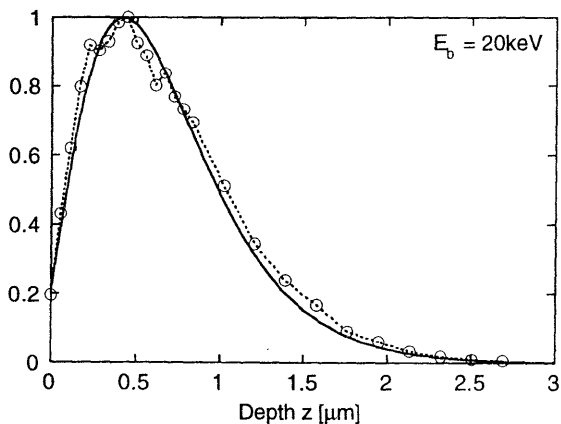
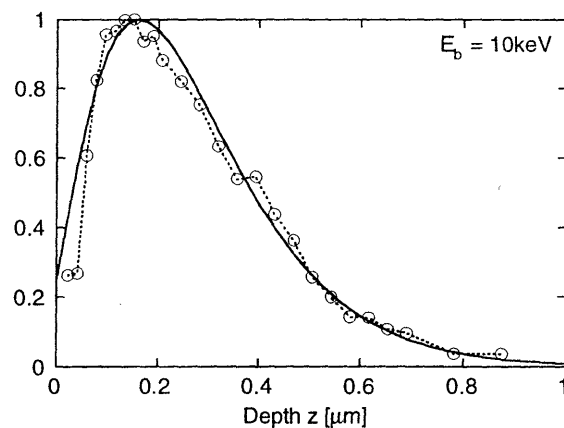
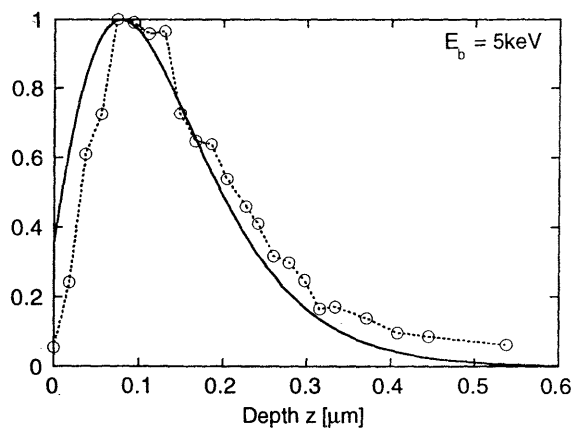


FIG. 12. Depth dependence of the e-h pair generation for beam energies of 5, 10, 20, and 40 keV, as measured (circles joined by dotted line) and as predicted by the analytical function of equations (1) and (2).

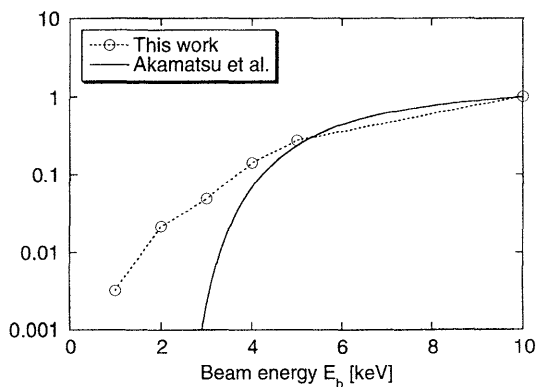


FIG. 13. Dependence on the beam energy of the CL intensity for a depth of 100 nm and a detector width of 50 nm, as measured in this work (circles joined by dotted line) and as predicted by Akamatsu *et al.* (plain line).

approximately 50 nm. The second reason is that even an electron beam with a small energy will be able to penetrate and spread into the material with more efficiency than predicted by the habitual penetration ranges: the theoretical penetration of 10 nm at 1 keV (evaluated with the Grün range) is not realistic. This fact is supported by Fig. 13, which compares the measured CL intensity for a depth z of 100 nm and the theoretical intensity after Akamatsu *et al.* for energies

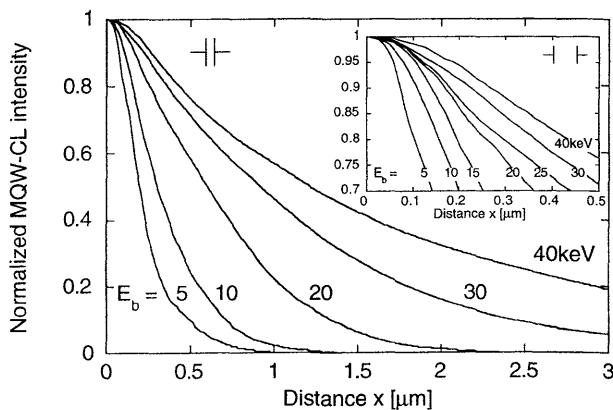


FIG. 14. Lateral dependence of the MQW-CL intensity as a function of the distance x to the MQW, for beam energies of 5, 10, 20, 30, and 40 keV. The intensity at $x=0$ is fixed to 1. The coordinates are the same as in Fig. 3, and the marker indicates the resolution (50 nm). The inset shows a blow-up for distances inferior to 0.5 μm .

between 1 and 10 keV. The measured intensity is orders of magnitude higher than predicted for energies lower than 4 keV. So we may conclude that all expressions that describe the interaction between the sample and the beam underesti-

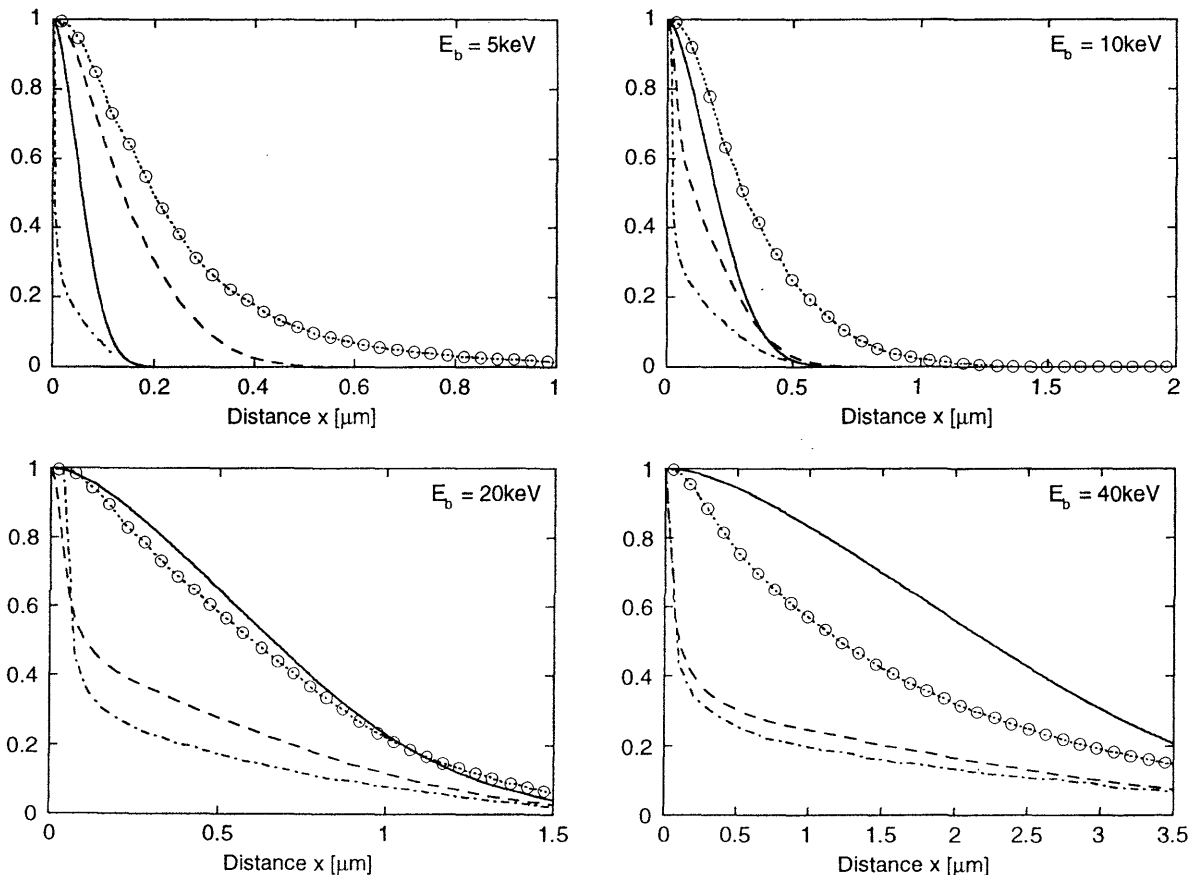


FIG. 15. Lateral dependence of the e-h pair generation for beam energies of 5, 10, 20, and 40 keV; as predicted by the expression of Akamatsu *et al.* (plain line), by the expression of Konnikov *et al.* (dashed line), by the simulation program MC-SET (dash-dotted line) and as measured in this work (circles joined by dotted line)

mate greatly t
and give a mis
energies.

V. LATERAL A. Experiments

The results of the
previous article
In Fig. 1, the
various beam
position of the
3). As expected,
ume increase
small distance
in the inset (a
artifact, and v

B. Comparison

As for the
ments with th
a greater lat
et al. curves
Werner *et al.*
an energy-in
lateral depen
lateral spread
following th
*et al.*¹⁵ are s
given by the

Figure 1
40 keV (circ
curves corre
Konnikov *et al.*
None of
for all beam
sion of Ko
match by fa
nearly inde
previous st
given by Al

C. Analytical

As for the
tion of the
good approx
Gaussians:

$$I(x) = I_0 \exp(-x/\lambda)$$

with x (in
 μm), and λ

The analytical
polynomial

$$A = 1.0$$

The width

mate greatly the penetration of the electrons at low energies and give a misleading picture of e-h pairs generation at small energies.

V. LATERAL DEPENDENCE

A. Experimental results

The results on the lateral dependence are reported in a previous article.²¹ We present here the main conclusions.

In Fig. 14, the obtained CL profiles are presented for various beam energies, normalized at $x=0$ ($x=0$ is set at the position of the MQW, with the same coordinates as in Fig. 3). As expected, the lateral extension of the generation volume increases with the beam energy. This is also true for small distances ($x \leq 0.5 \mu\text{m}$) from the detector, as is shown in the inset of Fig. 14. The latter feature is not a measure artifact, and was not observed in previous studies.^{8,9}

B. Comparison with previous studies

As for the depth dependence, we compare our measurements with the results of previous studies. Figure 1(b) shows a greater lateral spreading of the beam for the Akamatsu *et al.* curves than for the predictions of Konnikov *et al.*⁹ and Werner *et al.*⁸ The expression of Oelgart and Werner⁷ uses an energy-independent function for the central part of the lateral dependence and does not consider the variation of the lateral spreading of the beam with the beam energy. In the following the expressions of Konnikov *et al.* and Akamatsu *et al.*¹⁵ are selected for the comparison, along with the results given by the Monte Carlo simulation program MC-SET.²³

Figure 15 displays the measured profiles at 5, 10, 20, and 40 keV (circles joined by dotted line) together with the curves corresponding to the expression of Akamatsu *et al.*, Konnikov *et al.*, and MC-SET's results.

None of the models fits well with the measured profiles for all beam energies. The profiles derived from the expression of Konnikov *et al.* (and MC-SET's results) do not match by far our measurements, since we do not observe a nearly independent needle-like peak around $x=0$ like most previous studies.⁷⁻⁹ The only approaching estimation is given by Akamatsu's model between 10 keV and 20 keV.

C. Analytical function

As for the depth dependence, an analytical approximation of the experimental shape of the profiles is possible. A good approximation is obtained here with a sum of two Gaussians:

$$I(x) = A \exp\left(-\frac{x^2}{2\sigma_1^2}\right) + (1-A) \exp\left(-\frac{x^2}{2\sigma_2^2}\right) \quad (5)$$

with x (in μm), σ_1 , σ_2 the widths of the Gaussians (in μm), and A the amplitude of the first Gaussian.

The amplitude A of the first Gaussian can be written as a polynomial of third order:

$$A = 1.07 - 0.093E_b + 3.55 \times 10^{-3}E_b^2 - 4.01 \times 10^{-5}E_b^3 \quad (6)$$

The widths are found to follow a law in

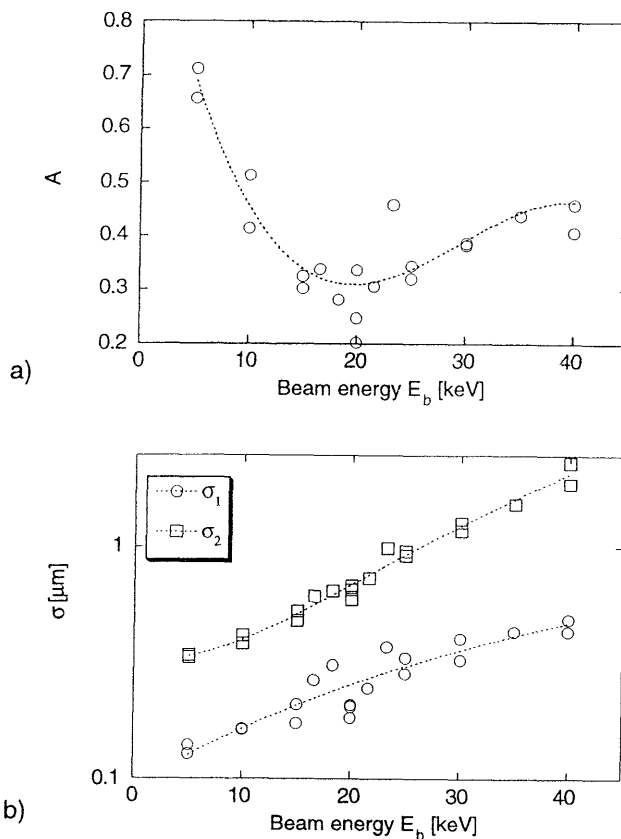


FIG. 16. Dependence on the beam energy of the parameters A (a) and σ_1 , σ_2 (b) of the analytical function of equation (5) describing the lateral dependence measured in this work, along with the curves (dotted line) corresponding to equations (6) (a) and (7) (b).

$$\sigma_i = a_i + b_i \times E_b^{c_i}, \quad i=1,2 \quad (7)$$

with E_b , the beam energy, (in keV), and

$$a_1 = 0.1, \quad b_1 = 0.0035, \quad c_1 = 1.25;$$

$$a_2 = 0.32, \quad b_2 = 0.0004, \quad c_2 = 2.25.$$

Figure 16 shows the dependence of the amplitude (a) and of the widths (b) with the beam energy, together with the curves corresponding to equations (6) and (7).

The experimental profiles for 5, 10, 20, and 40 keV along with the curve corresponding to equations (5) to (7) are displayed in Fig. 17, to indicate again the validity of the analytical function for our measurements. The overall coincidence between analytical and experimental curves is very good, apart from the 40 keV curve where a slight deviation is observed for medium distances.

The first Gaussian is seen as the contribution to the carrier generation of the primary electrons after no or only a few scattering events, and the second Gaussian as the contribution of the primary electrons after multiple scattering events. The width of the two Gaussians increases with energy, because the energy loss per distance decreases with energy: a high energetic electron will penetrate deeper and further away from the beam axis into the sample than a low energetic one. The first Gaussian will be less sensitive than the second one to this effect, since the electrons cannot travel too

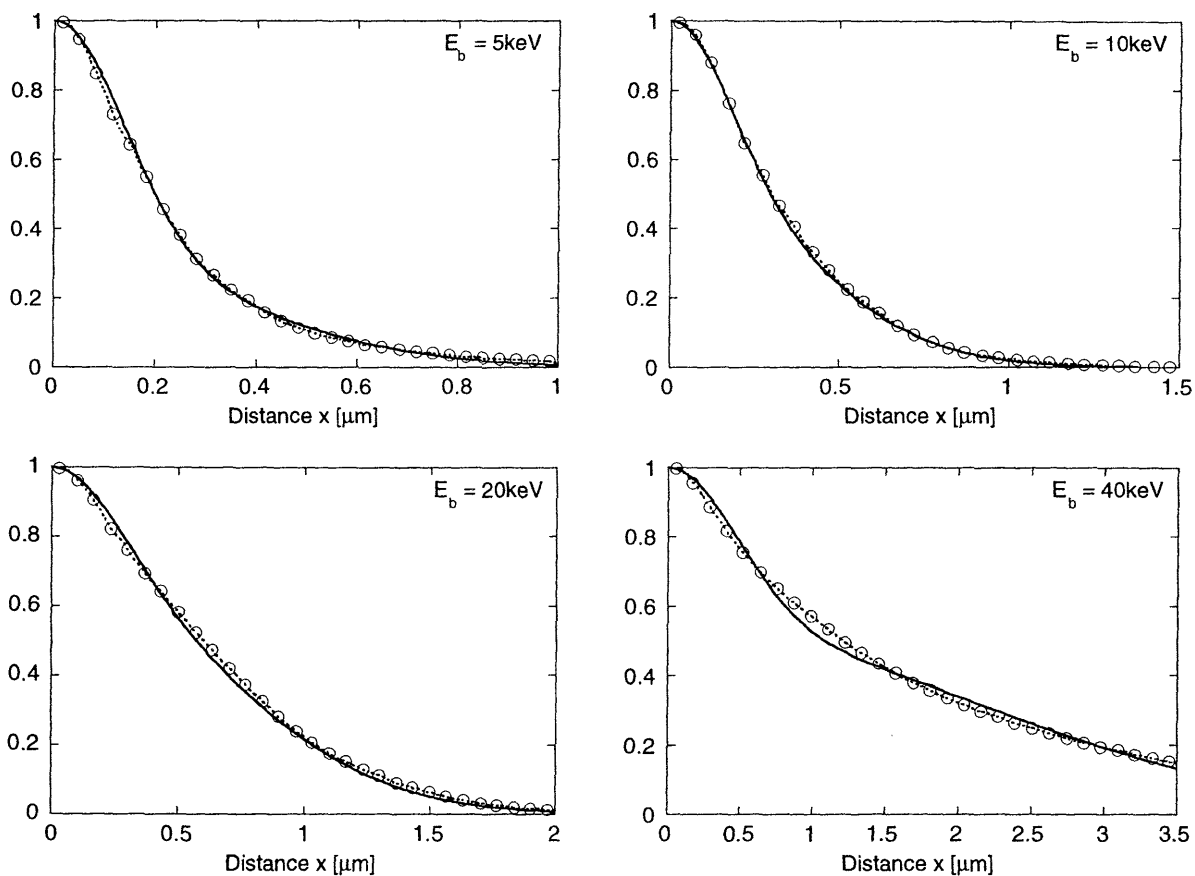


FIG. 17. Lateral dependence of the e-h pair generation for beam energies of 5, 10, 20, and 40 keV, as measured (circles joined by dotted line) and as predicted by the analytical function of equations (5)–(7).

far from the beam axis after only a few elastic scatterings only: This is supported by our measurements since $c_2 > c_1$ in Eq. (7).

A feature similar with the results on the depth dependence is that the width of the two Gaussians will not tend towards zero with decreasing energy. For the first Gaussian, this is due to the finite diameter of the beam as well as to the size of the detector. For the second Gaussian, the beam will spread into the sample even at low energies, but its contribution will be very small. Equations (6) and (7) cannot be expected to hold for energies below 1 keV, but the statement we make at the end of section IV C on the inaccuracy of existing functions at low energies holds also for the lateral dependence.

VI. CONCLUSION

The spatial distribution of e-h pairs generated by the electron beam of a SEM in $Al_{0.4}Ga_{0.6}As$ is measured for different beam energies. The use of a MQW structure for the detection of the created minority carriers by their radiative recombination makes possible a direct determination of their distribution, without the contribution of carriers differing out of and into the detector. The employed method can be applied to other III-V and II-VI semiconductors, provided that

an internal detector can be grown in the material, and provided that the CL emission of the detector can be isolated from a possible background.

Our results are compared with available analytical functions: the model of Akamatsu *et al.* fits our measurements quite well for energies superior to 10 keV. All analytical functions however are inaccurate for lower beam energies. We therefore provide two analytical functions describing our measurements on the depth, respectively lateral, dependence of the generation.

We believe that this method will yield further information on the generation volume and will prove a help for the quantitative interpretation of EBIC and CL measurements.

ACKNOWLEDGMENTS

We would like to thank B. Garoni, B. Senior, G. Peter and D. Laub at the Centre Interdépartmental de Microscopie Electronique (CIME-EPFL) for the expert technical support with the microscopes and the help with sample preparation. We are also indebted to G. Oelgart (Leipzig University) for valuable discussions, to F. Morier-Genoud (IMO-EPFL) for growing and providing the sample, and to A. Gustafsson (IMO-EPFL) for the use of the MC-SET program. This work is part of the "OPTIQUE" priority program of the board of the Swiss Federal Institutes for Technology.

- 1 B. G. Yacobi and D. B. Holt, *Cathodoluminescence Microscopy of Inorganic Solids* (Plenum, New York, 1990).
- 2 H.J. Leamy, *J. Appl. Phys.* **53**, R51 (1982).
- 3 A.E. Grün, *Z. Naturforsch.* **12a**, 89 (1957).
- 4 A. Cohn and G. Caledonia, *J. Appl. Phys.* **41**, 3767 (1970).
- 5 T.E. Everhart and P.H. Hoff, *J. Appl. Phys.* **42**, 5837 (1971).
- 6 G. Oelgart and H. Scholz, *Phys. Status Solidi A* **75**, 547 (1983).
- 7 G. Oelgart and U. Werner, *Phys. Status Solidi A* **85**, 205 (1984).
- 8 U. Werner, F. Koch, and G. Oelgart, *J. Phys. (Paris) D* **21**, 116 (1988).
- 9 S.G. Konnikov, V.A. Solev'ev, V.E. Umanskii, and V.M. Chistyakov, *Sov. Phys. Semicond.* **21**, 1229 (1988).
- 10 C. Donolato, *Phys. Status Solidi A* **65**, 649 (1981).
- 11 C.A. Klein, *J. Appl. Phys.* **39**, 2029 (1968).
- 12 D.B. Wittry and D.F. Kyser, *J. Appl. Phys.* **36**, 1387 (1965).
- 13 C.J. Wu and D.B. Wittry, *J. Appl. Phys.* **49**, 2827 (1978).
- 14 H.-J. Fitting, H. Glaefcke, and W. Wild, *Phys. Status Solidi A* **43**, 185 (1977).
- 15 B. Akamatsu, P. Henoc, and R. B. Martins, *J. Microsc. Spectr. Electron.* **14**, 12a (1989).
- 16 C. Donolato, *Solid-State Electron.* **25**, 1077 (1982).
- 17 K.L. Luke, O. von Roos, and L.J. Cheng, *J. Appl. Phys.* **57**, 1978 (1984).
- 18 K.L. Luke, *J. Appl. Phys.* **75**, 1623 (1994).
- 19 C. Donolato, *J. Appl. Phys.* **76**, 959 (1994).
- 20 B. Sieber, *Mat. Sci. Eng. B* **24**, 35 (1994).
- 21 D. Araújo, J.-M. Bonard, G. Oelgart, J.-D. Ganière, F. Morier-Genoud, and F.-K. Reinhart, *Mat. Sci. Eng. B* **24**, 124 (1994).
- 22 A.M. Huber, G. Laurencin, and M. Razeghi, *J. Phys. (Paris)* **44** C4-409 (1983).
- 23 D.B. Holt and E. Napchan, *Scanning* **16**, 78 (1994).

5

is predicted

and pro-
isolated

cal func-
urements
analytical
energies.
ibing our
pendence

informa-
p for the
ements.

G. Peter
roscopie
l support
paration.
rsity) for
PFL) for
ustafsson
his work
board of

nard et al.